2023-01

Three-layer model with absorption for conservative estimation of the maximum acoustic transmission coefficient through the human skull for transcranial ultrasound stimulation

Attali, D

http://hdl.handle.net/10026.1/20189

Three-layer model with absorption for conservative estimation of the maximum acoustic transmission coefficient through the human skull for transcranial ultrasound stimulation

David Attali [a, b, 1], Thomas Tiennot [a, 1], Mark Schafer [c], Elsa Fouragnan [d, p], Jérôme Sallet [e], Charles F Caskey [f], Robert Chen [g, h], Ghazaleh Darmani [h], Ellen J. Bubrick [i], Christopher Butler [j], Charlotte J Stagg [k], Miriam Klein-Flügge [k, l], Lennart Verhagen [m], Seung-Schik Yoo [n], Kim Butts Pauly [o, 1], Jean-Francois Aubry [a, 1, *]

[a] Physics for Medicine Paris, Inserm U1273, ESPCI Paris, CNRS UMR8063, PSL University, Paris, France
[b] Pôle Paris 16 (Secteurs 17-18) et Pôle Neuro Sainte-Anne, Centre Hospitalier Sainte-Anne, GHU Paris Psychiatrie & Neurosciences, Université Paris Cité, Paris, France
[c] School of Biomedical Engineering, Science and Health Systems, Drexel University, Philadelphia, PA, USA
[d] Brain Research Imaging Center and School of Psychology, University of Plymouth, Plymouth, UK
[e] Univ Lyon, Université Lyon 1, Inserm, Stem Cell and Brain Research Institute U1208, Bron, France
[f] Vanderbilt University Institute of Imaging Sciences, VU Medical Center, Nashville, TN, United States
[g] Division of Neurology, Department of Medicine, University of Toronto, Canada
[h] Krembil Research Institute, University Health Network, Toronto, Ontario, Canada
[i] Brigham and Women's Hospital, Harvard Medical School, Department of Neurology, 75 Francis St., Boston, MA, USA
[j] Department of Brain Sciences, Imperial College London, 9th Floor, Sir Michael Uren Hub, 86 Wood Lane, London, W12 0BZ, UK
[k] Wellcome Centre for Integrative Neuroimaging (WIN), Centre for Functional MRI of the Brain (FMRIB), University of Oxford, Nuffield Department of Clinical Neurosciences, Level 6, West Wing, John Radcliffe Hospital, Oxford OX3 9DU, UK
[l] Wellcome Centre for Integrative Neuroimaging (WIN), Department of Experimental Psychology, University of Oxford, Tinsley Building, Mansfield Road, Oxford OX1 3TA, UK
[m] Donders Institute for Brain, Cognition and Behaviour, Radboud University, 6525 GD Nijmegen, the Netherlands
[n] Brigham and Women's Hospital, Harvard Medical School, Department of Radiology, 75 Francis St., Boston, MA, USA
[o] Stanford University, Department of Radiology, Stanford CA, 94305, USA
[p] School of Psychology, Portland Square, Plymouth PL4 8AA, UK

ABSTRACT

Transcranial ultrasound stimulation (TUS) has been shown to be a safe and effective technique for non-invasive superficial and deep brain stimulation. Safe and efficient translation to humans requires esti-mating the acoustic attenuation of the human skull. Nevertheless, there are no international guidelines for estimating the impact of the skull bone. A tissue independent, arbitrary derating was developed by the U.S. Food and Drug Administration to take into account tissue absorption (0.3 dB/cm-MHz) for diagnostic ultrasound. However, for the case of transcranial ultrasound imaging, the FDA model does not take into account the insertion loss induced by the skull bone, nor the absorption by brain tissue. Therefore, the estimated absorption is overly conservative which could potentially limit TUS applications if the same guidelines were to be adopted. Here we propose a three-layer model including bone ab-sorption to calculate the maximum pressure transmission through the human skull for frequencies ranging between 100 kHz and 1.5 MHz. The calculated pressure transmission decreases with the fre-quency and the thickness of the bone, with peaks for each thickness corresponding to a multiple of half the wavelength. The 95th percentile maximum transmission was calculated over the accessible surface of 20 human skulls for 12 typical diameters of the ultrasound beam on the skull surface, and varies between 40% and 78%. To facilitate the safe adjustment of the acoustic pressure for short ultrasound pulses, such as transcranial imaging or transcranial ultrasound stimulation, a table summarizes the maximum pressure transmission for each ultrasound beam diameter and each frequency.

1. Introduction

Transcranial Ultrasound Stimulation (TUS) allows for the stimulation of superficial [1–9] and deep [10–13] regions with unparalleled resolution for a non-invasive technique [14,15]. As is the case for any biomedical use of ultrasound waves, it also comes with potential risks that must be anticipated to ensure patient safety.

There are two main risks associated with the application of TUS, namely thermal and mechanical bioeffects [16,17]. Concerning thermal bioeffects, mechanical energy can be transferred into thermal energy through viscous absorption leading to tissue heating [18–21]. This article is focused on mechanical bioeffects, which concern mainly the risk of acoustic cavitation [22–26]. Currently, there are no established guidelines for the safe application of ultrasonic neuromodulation in humans. Nevertheless, dedicated recommendations could be developed based on existing guidelines for diagnostic ultrasound from regulatory bodies like the U.S. Food and Drug Administration (FDA) [27].

The Mechanical Index (MI) was introduced to inform the clinical user about the relative risk from mechanical effects [28]. It is defined by the spatial-peak value of the peak rarefactional pressure at the location where the pulse intensity integral is maximum. The location of the maximum intensity is often located at the focal point [29], deep into tissues, so the FDA developed a "derating" factor to account for the attenuation of the ultrasound beam during the propagation into tissues. For simplicity of implementation, a single arbitrary derating factor is used for all clinical situations. However, the derating implemented by the FDA ($0.3 \, \mathrm{dB \, cm^{-1} \, MHz^{-1}}$) is lower than the attenuation of any solid tissue in the body and does not take into account the insertion loss induced by the skull bone [30–34]. The current MI implementation thus overestimates the actual pressure inside the brain and is overconservative for transcranial applications both diagnostic and neuromodulatory. Adding a conservative maximum transmission coefficient of the pressure amplitude through the skull to the MI would partially account for this overestimation. Further, incorporating a more realistic value of tissue absorption would also improve the pressure estimation.

Here, we introduce a conservative analytical model to estimate the maximum possible transmission through a human skull at a given frequency and a given thickness of the skull, a model where all parameters tend towards the worst-case scenario. We then applied this model to the entire surface of 20 human skulls for a [100 kHz - 1.5 MHz] range of ultrasound frequencies. The pressure transmission coefficients were calculated at each frequency for a set of ultrasound beam diameters on the skull surface ranging between 5 mm and 100 mm (5 mm, then 10–100 mm with 10 mm increments), at 100,000 locations uniformly distributed at the surface of the skull. The maximum transmission computed over the 1.4 M locations is compared to experimental data published in the literature.

2. Methods

2.1. Analytical model of ultrasonic transmission

The objective of the model is to estimate the maximum pressure transmission through a human skull model. A 3-layer model is proposed, with 3 impedances representing the skin, skull and brain (Fig. 1). A harmonic plane wave at normal incidence is considered.

In the case of a lossless media, an analytical solution can be calculated by considering 5 waves: the contra propagating waves (incident and reflected) in medium 1 and 2, and the transmitted wave in medium 3 [35]. Taking into account the boundary conditions, it can be shown that the intensity transmission coefficient is given by Ref. [36]:

$$T = \frac{4Z_1 Z_3}{(Z_1 + Z_3)^2 \, cos^2 k_2 L + (Z_2 + Z_1 Z_3/Z_2)^2 \, sin^2 k_2 L} \tag{1}$$

where k_2 is the wave vector in the second medium.

We propose here to take into account the attenuation of the wave in the skull. The attenuation is modeled by a homogenous absorption coefficient α (in $\mathrm{Np.m^{-1}}$) such that a plane wave propagating along a distance L is given by:

$$P(x = L) = P(x = 0)e^{j(\omega t - kL)}e^{-\alpha L} \tag{2}$$

where $P(x = 0)$ is the plane wave at the reference position, ω the pulsation of the wave, and k the wave vector.

The acoustic pressure $P_3(x = L)$ in the third medium (the brain) at the location of the third interface is the sum of all the successive reflected waves at the two interfaces that were transmitted in the third medium:

$$P_3(x = L) = t_{12}t_{23}P_0 e^{j(\omega t - k_2 L)}e^{-\alpha L} + t_{12}t_{23}r_{23}r_{21}P_0 e^{j(\omega t - 3k_2 L)}e^{-3\alpha L}$$
$$+ t_{12}t_{23}r_{23}r_{21}r_{23}r_{21}P_0 e^{j(\omega t - 5k_2 L)}e^{-5\alpha L} + \ldots \tag{3}$$

where $t_{ij} = \frac{2Z_j}{Z_i + Z_j}$ is the pressure transmission coefficient of a wave propagating from medium i to medium j, and where $r_{ij} = \frac{Z_j - Z_i}{Z_j + Z_i}$ is the pressure reflection coefficient of a wave propagating from medium i to medium j. Equation (3) can be rewritten as:

$$P_3(x = L) = t_{12}t_{23}P_0 e^{j(\omega t - k_2 L)}e^{-\alpha L}$$
$$\left(1 + r_{23}r_{21}e^{-2jk_2 L}e^{-2\alpha L} + (r_{23}r_{21})^2 e^{-4jk_2 L}e^{-4\alpha L} + \ldots\right) \tag{4}$$

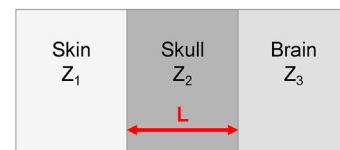where the sum of the geometrical series can be calculated as:

Fig. 1. A 3-layer model was used here, with 3 impedances reflecting the skin, skull and brain. The thickness of the skull (L), considered of homogenous composition, is used in the model.

$$P_3(x=L) = t_{12}t_{23}P_0 e^{j(\omega t - k_2 L)} e^{-\propto L} \left(\frac{1}{1 - r_{23}r_{21}e^{-2jk_2 L}e^{-2\propto L}} \right) \quad (5)$$

The pressure transmission coefficient is thus given by:

$$t = \frac{4Z_2 Z_3 e^{-\propto L} e^{-jk_2 L}}{(Z_1 + Z_2)(Z_2 + Z_3) - (Z_1 - Z_2)(Z_3 - Z_2)e^{-2\propto L}e^{-2jk_2 L}} \quad (6)$$

which can be finally written as:

$$t = \frac{4Z_2 Z_3 e^{-\propto L}}{(Z_1 + Z_2)(Z_2 + Z_3)e^{jk_2 L} - (Z_1 - Z_2)(Z_3 - Z_2)e^{-2\propto L}e^{-jk_2 L}} \quad (7)$$

A linear relationship of the absorption coefficient in the bone with the ultrasound frequency f was chosen [29,37]:

$$\propto = \beta f \quad (8)$$

which leads to the transmission coefficient as a function of frequency:

$$t = \frac{4Z_2 Z_3 e^{-\beta f L}}{(Z_1 + Z_2)(Z_2 + Z_3)e^{jk_2 L} - (Z_1 - Z_2)(Z_3 - Z_2)e^{-2\beta f L}e^{-jk_2 L}} \quad (9)$$

This formula can be used to compute the intensity transmission coefficient. In a lossless media ($\alpha = 0$), the model corresponds to Equation (1) (see supplementary materials).

The impedances of the three media were calculated from the density and speed of sound values shown in Table 1.

There is currently no consensus on the modeling of the ultrasonic attenuation in the skull. Vastly different values have been measured or estimated, ranging from 83 to 515 Np.m^{-1}.MHz^{-1} [38]. In order to estimate the maximum transmission coefficients, the lowest value of attenuation in the skull was used, i.e., 83 Np.m^{-1}.MHz^{-1} [38–40]. We assumed a linear relationship with frequency even though more complex models have been published [41]. Overall, this model aims at estimating the transmission coefficient as a function of the ultrasound frequency and the thickness of the skull.

2.1.1. Application of the 3-layer model with absorption to 20 human skulls

Local variations in the thickness of the skull have an impact on the transmission coefficient when applied to an ultrasound beam passing through the skull with a given diameter. Thus, to define a maximum transmission coefficient by ultrasound frequency and

Table 1
Density, sound speed, impedance [42] and attenuation [38–40] used in the analytical model. The lowest value of attenuation in the skull was used. Attenuation for skin and brain tissue are not relevant for the current modeling of the attenuation of the skull.

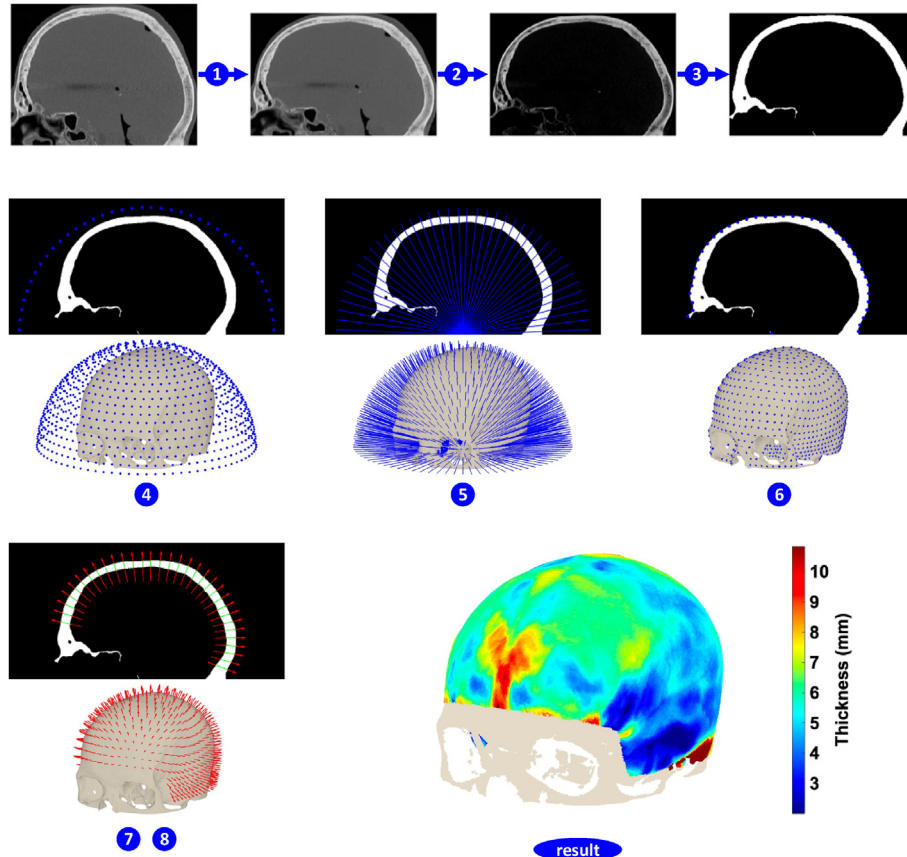|	Density kg.m^{-3}	Sound speed m.s^{-1}	Impedance rayl	Attenuation Np.m^{-1}.MHz^{-1}
Skin	1116	1537	1.7	–
Skull	1990	2930	5.8	83
Brain	1041	1562	1.6	–

Fig. 2. Thickness computation of skull #3 following the eight steps described in the Methods. For representation purposes in step 4 to 7, only 1.000 points (instead of 100.000) have been used for this figure.

beam diameter on the skull surface, this analytical model was applied on the whole surface of twenty human skulls.

Twenty computed tomography (CT) scans of human skulls from previous studies [43] were processed in Matlab R2021b to determine their thickness with the following steps (Fig. 2):

(1) Isotropic interpolation of the CT image at a resolution of 0.3*0.3*0.3 mm.
(2) Minimal thresholding by setting all negative values to zero.
(3) Creation of a skull mask with the voxels above a threshold value defined for each skull by the Otsu method [44] and morphological closing on this binary image using a 3D spherical structuring element with a 3 mm radius.
(4) Creation of a semi-sphere of 100.000 points around the skull.
(5) Ray tracing between the center of this sphere and each of its points.
(6) Determination of the intersecting points between the external surface of the skull and these 100.000 rays.
(7) Computation of the normal vector to the surface at each intersecting point; consideration of the vectors from a manually determined ROI including the entire skull except the facial skeleton and skull base.
(8) At each of these points, computation of the thickness of the skull at high resolution (0.03 mm) with minimum and maximum limits of 1 mm [45,46] and 20 mm [47], respectively.

The analytical model previously described was applied to each of these outer surface points for ultrasound frequencies between 100 kHz and 1.5 MHz. Finally, at each of these points, these single values were averaged across all points within diameters between 5 mm and 100 mm to model different ultrasound beam diameters on the skull surface (Fig. 3).

The maximum transmission coefficient by ultrasound frequency and beam diameter is defined as the FDA-recognized standard 95th percentile (AAMI/ANSI HE75 [48]) of the values of all points of all 20 human skulls.

2.1.2. Comparison with experimental values

The transmission coefficient values from this conservative model were compared to experimental values found in the scientific literature using different ultrasound frequencies and ultrasound beam diameters on the skull surface. The literature included transcranial ultrasound in general (neuromodulation papers or not). In any case these articles had to include (i) experimentally measured pressure transmission ratio through the skull, (ii) ultrasound frequency, and (iii) information to calculate the ultrasound beam diameter on the skull surface.

3. Results

3.1. Transmission coefficient in the [100kHz-1.5 MHz] frequency range

Fig. 2 displays the pressure transmission coefficient as a function of the ultrasound frequency and the thickness of the skull.

Globally, the transmission coefficient decreases with both the frequency and the thickness of the skull. Peaks appear regularly when the thickness of the skull is equal to a multiple of half the ultrasonic wavelength in the skull.

3.1.1. Maximum transmission coefficient by ultrasound frequency and beam diameter on the skull surface

The analytical model was then applied to each point of 20 human skulls, corresponding to a total of 1.465.136 points (Fig. 4A). The Otsu threshold values ranged from 446 HU to 698 HU (mean ± SD: 564 ± 77 HU). Fig. 4B illustrates the impact of geometrical averaging for 20 mm and 60 mm beam diameters.

The maximum transmission coefficients of acoustic pressure vary from 40% to 78%. These coefficients are displayed by ultrasound frequency and ultrasound beam diameter on the skull surface in Fig. 5.

3.1.2. Comparison with experimental values from the scientific literature

Seven publications [6,12,40,49−52] with experimental measurements of transmission coefficients were selected for comparison with the model provided here. Ultrasound frequency, beam diameter on the skull surface, and sound pressure transmission coefficient are presented in Table 2 for each of these studies. As would be expected from a conservative model, the values given by the model are consistently higher by some margin than those measured experimentally.

4. Discussion

We introduce a simple model that provides a reasonable estimate of the maximum transmission of pressure amplitude through a human skull. This estimation is essential to anticipate the mechanical risks related to ultrasound. The literature is not unanimous on the global attenuation coefficients to be applied to an incident ultrasound beam, with a significant variability between models [38].

More complex models have been introduced in the past to simulate the propagation of an ultrasound wave through a human skull [53−55]. Such refined models could be used to estimate the in-situ pressure in the brain for a given transducer and a given treatment geometry [3,56], provided the user can run the corresponding simulations. Nevertheless, not all users involved in transcranial ultrasound have access to such numerical models. Also, to experimentally measure the acoustic pressure through a human skull requires a fine and demanding methodology and is also not within the reach of all users. Moreover, depending on the morphology and thickness of the skull, the transmission coefficients differ. These differences are not straightforward: the thinnest regions do not necessarily correspond to the highest
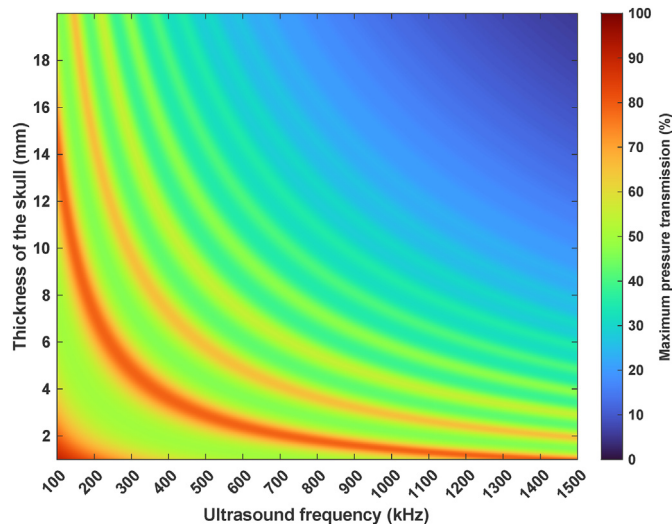

Fig. 3. Pressure transmission as a function of ultrasound frequency and thickness of the skull, using the 3-layer analytical model.
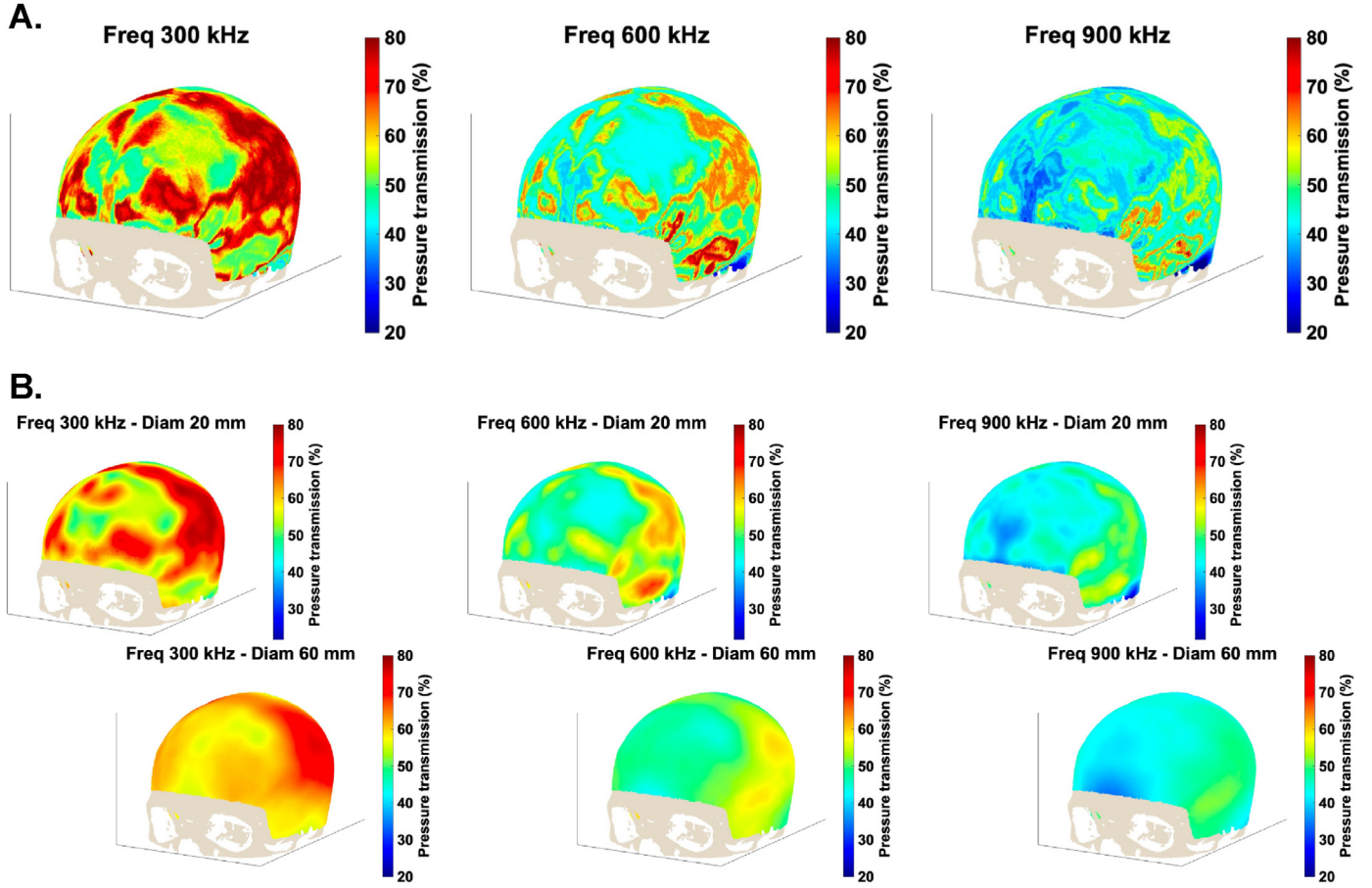
Fig. 4. Pressure transmission coefficient computation for skull #3 for a range of ultrasound frequencies (300, 600 and 900 kHz in A.) and a range of ultrasound beam diameters on the skull surface (20 and 40 mm in B.).

transmission. Indeed, the skull thicknesses associated with the highest transmission coefficients depend on the ultrasound frequency as shown in Fig. 4.

Fig. 5. Maximum pressure transmission as a function of ultrasound frequency and ultrasound beam diameter on the skull surface. The values shown here are the 95th percentile of all points of all 20 skulls. The "0 mm" line corresponds to the single values not averaged over the ultrasound beam diameter.

The main objective of this work was to provide a conservative and yet realistic model to estimate the maximum expected pressure transmission and thus adjust the acoustic pressure in a conservative way. The following choices were made to introduce a conservative worst-case scenario model:

(i) all the ultrasonic waves were assumed to be normal to the surface of the skull on both the outer and inner tables [40],
(ii) the defocusing impact of the skull was neglected, and only the transmission amplitude was considered, assuming that a perfect phase aberration correction was applied to the transducer [57–59],
(iii) the skull was considered of homogenous composition and a low value of ultrasound attenuation in the skull was used. The diploe is known to attenuate ultrasound beams more because of its additional scattering [30,31]. Nevertheless, cortical bone only was considered and is used as the lower bound of the absorption coefficient in cortical cranial bone reported in the literature.
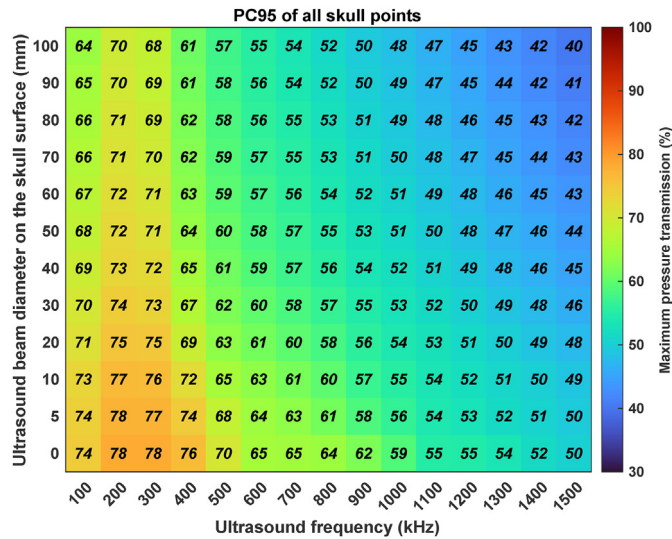
Following the first application of ultrasound stimulation to non-human primates [1], TUS has been rapidly translated to human volunteers [3,6,12,13,56,60–63]. As no guidelines are currently available for safe and effective TUS, various methods have been used to estimate the acoustic transmission and thus adjust the acoustic pressure of TUS devices. The most conservative approach consisted in completely neglecting the tissue absorption and using the acoustic pressure measured at the focus in free water [62].

Table 2
Comparison between values of pressure transmission through the skull from the scientific literature and from this study. Because of the conservative worst-case scenario model, values from this study are higher than experimental ones.

Authors	Values from the scientific literature			Corresponding values in this study		
	US frequency	US beam diameter on the skull surface	**Pressure transmission**	US frequency	US beam diameter on the skull surface	**Maximum pressure transmission**
White et al. *(2006)*	272 kHz	25 mm	**61%**	300 kHz	30 mm	**73%**
	548 kHz	25 mm	**48%**	600 kHz	30 mm	**60%**
	840 kHz	25 mm	**41%**	900 kHz	30 mm	**55%**
Marsac et al. *(2017)*	800 kHz	92 mm	**32%**	800 kHz	100 mm	**52%**
	1.3 MHZ	92 mm	**16%**	1.3 MHZ	100 mm	**43%**
Gimeno et al. *(2019)*	270 kHz	54 mm	**50%**	300 kHz	60 mm	**71%**
Riis et al. *(2021)*	500 kHz	28.5 mm	**46%**	500 kHz	30 mm	**62%**
Chen et al. *(2022)*	150 kHz	43 mm	**47%**	200 kHz	50 mm	**72%**
	350 kHz	44 mm	**33%**	400 kHz	50 mm	**64%**
	500 kHz	28 mm	**36%**	500 kHz	30 mm	**62%**
	750 kHz	26 mm	**17%**	800 kHz	30 mm	**57%**
	1 MHz	27 mm	**12%**	1 MHz	30 mm	**53%**
	1.5 MHz	27 mm	**4%**	1.5 MHz	30 mm	**46%**

Other teams used the ultra-conservative constant derating used by the FDA for all human tissues (0.3 dB cm^{-1} MHz^{-1}) to estimate the transcranial maximum in situ acoustic pressure [13,63]. Others performed numerical simulations of the propagation of the acoustic waves through the skull [3,56]. Finally, some investigators used the transmission coefficient measured experimentally on one fragment of human parietal bone [61], or the experimental value of the transmission coefficient published by other research teams [60].

We offer here a model that can be used in the absence of subject specific modeling. The model is currently based on the analysis of 20 human skulls. Fig. 5 can be used as a guide to derate the maximum pressure in the brain with a conservative model.

For example, consider here a 1 MHz transducer with 8 cm active diameter and a 12 cm radius of curvature used to achieve deep brain TUS (6 cm deep in the brain). We assume that a peak negative pressure of 1 MPa was measured in free water with a calibrated hydrophone. As the focal point is 6 cm deep in the brain, it implies that the skull bone is 12 - 6 = 6 cm away from the transducer. From a simple geometric consideration with the skull surface halfway between the transducer and the geometrical focus, the diameter of the beam intersecting the skull is thus 8/2 = 4 cm. Based on Fig. 5, the maximum transmission through the skull is 52%. The maximum pressure at focus will thus be 0.52 MPa. The pressure additionally suffers from the attenuation of the 6 cm propagation in the brain. The attenuation in the brain is higher than other soft tissues, and a reasonable value is 0.5 dB cm^{-1} MHz^{-1} [42]. It corresponds to an additional attenuation of 3 dB, corresponding to a pressure attenuation of 30%. For the transducer considered here the maximum pressure in the brain would be estimated to be 0.52 MPa * $(1-0.3)$ = 0.52 MPa * 0.7 = 0.36 MPa. Using the existing FDA derating approach for diagnostic ultrasound, 1 MPa at 6 cm deep at 1 MHz would produce an MI of 0.81. But the better estimate within brain tissue, after bone attenuation would be 0.36.

One limitation of this article is the number of skulls included in the study. The inclusion of 20 human skulls establishes a first proof of concept and introduces the impact of the size of the transducer. The results are in line with previously reported transmission coefficients but are not sufficient to set new standards. Further work will need to be performed to include more skulls and provide a more reliable value of the maximum transmission. The model could additionally be refined by taking into account the anatomical variability of the bones and differentiate the temporal, parietal and occipital bone attenuation. Nevertheless, the authors believe that

this paper provides the methodology for establishing reasonable conservative maximum transmission coefficients through human skulls. All the authors are active members of the safety committee of the ITRUSST consortium [64]. The committee intends to build upon the results presented here to provide recommendations for safe transcranial ultrasound stimulation. We believe that the maximum transmission coefficient will be key to assess the mechanical safety of TUS. The thermal safety must not be neglected and will be addressed separately.

5. Conclusions

The three-layer model with absorption introduced here led to the estimation of conservative values of maximum pressure transmission through human skulls that can be used to safely adjust the acoustic pressure for transcranial ultrasound. It can be directly applied for a safe use of transcranial diagnostic ultrasound provided the calculated Mechanical Index stays below the FDA recommendations. It must be kept in mind that thermal safety needs to be addressed separately to ensure a safe use of transcranial ultrasound. Further work will be conducted by the authors (members of the ITRUSST safety committee) to reach a consensus on how to extend these safety considerations to long sonications like the ones used for ultrasound neurostimulation.

CRediT authorship contribution statement

David Attali: Writing − original draft, Conceptualization, Methodology, Writing − review & editing. **Thomas Tiennot:** Writing − original draft, Conceptualization, Methodology, Writing − review & editing. **Mark Schafer:** Conceptualization, Writing − review & editing. **Elsa Fouragnan:** Conceptualization, Writing − review & editing. **Jérôme Sallet:** Conceptualization, Writing − review & editing. **Charles F Caskey:** Conceptualization, Writing − review & editing. **Robert Chen:** Conceptualization, Writing − review & editing. **Ghazaleh Darmani:** Conceptualization, Writing − review & editing. **Ellen J. Bubrick:** Conceptualization, Writing − review & editing. **Christopher Butler:** Conceptualization, Writing − review & editing. **Charlotte J Stagg:** Conceptualization, Writing − review & editing. **Miriam Klein-Flügge:** Conceptualization, Writing − review & editing. **Lennart Verhagen:** Conceptualization, Writing − review & editing. **Seung-Schik Yoo:** Conceptualization, Writing − review & editing. **Kim Butts Pauly:** Writing − original draft, Conceptualization, Methodology, Writing − review & editing.

Jean-Francois Aubry: Writing − original draft, Conceptualization, Methodology, Writing − review & editing, Supervision.

Declaration of competing interest

The authors declare that they have no known competing financial interests or personal relationships that could have appeared to influence the work reported in this paper.

Acknowledgements

Appendix A. Supplementary data

Supplementary data to this article can be found online at https://doi.org/10.1016/j.brs.2022.12.005.

References

[1] Deffieux T, Younan Y, Wattiez N, Tanter M, Pouget P, Aubry J-F. Low-intensity focused ultrasound modulates monkey visuomotor behavior. Curr Biol 2013;23:2430−3.

[2] Lee W, Kim H, Jung Y, Song I-U, Chung YA, Yoo S-S. Image-guided transcranial focused ultrasound stimulates human primary somatosensory cortex. Sci Rep 2015;5.

[3] Lee W, Kim H-C, Jung Y, Chung YA, Song I-U, Lee J-H, Yoo S-S. Transcranial focused ultrasound stimulation of human primary visual cortex. Sci Rep 2016;6.

[4] Wattiez N, Constans C, Deffieux T, Daye PM, Tanter M, Aubry J-F, Pouget P. Transcranial ultrasonic stimulation modulates single-neuron discharge in macaques performing an antisaccade task. Brain Stimul 2017;10:1024−31.

[5] Verhagen L, Gallea C, Folloni D, Constans C, Jensen DE, Ahnine H, Roumazeilles L, Santin M, Ahmed B, Lehericy S, Klein-Flügge MC, Krug K, Mars RB, Rushworth MF, Pouget P, Aubry J-F, Sallet J. Offline impact of transcranial focused ultrasound on cortical activation in primates. Elife 2019;8:e40541.

[6] Legon W, Sato TF, Opitz A, Mueller J, Barbour A, Williams A. Transcranial focused ultrasound modulates the activity of primary somatosensory cortex in humans. Nat Neurosci 2014;17. https://doi.org/10.1038/nn.3620.

[7] Yang P-F, Phipps MA, Newton AT, Chaplin V, Gore JC, Caskey CF, Chen LM. Neuromodulation of sensory networks in monkey brain by focused ultrasound with MRI guidance and detection. Sci Rep 2018;8:7993.

[8] Mueller J, Legon W, Opitz A, Sato TF, Tyler WJ. Transcranial focused ultrasound modulates intrinsic and evoked EEG dynamics. Brain Stimul 2014;7:900−8.

[9] Pouget P, Frey S, Ahnine H, Attali D, Claron J, Constans C, Aubry J-F, Arcizet F. Neuronavigated repetitive transcranial ultrasound stimulation induces long-lasting and reversible effects on oculomotor performance in non-human primates. Front Physiol 2020;11:1042.

[10] Folloni D, Verhagen L, Mars RB, Fouragnan E, Constans C, Aubry J-F, Rushworth MFS, Sallet J. Manipulation of subcortical and deep cortical activity in the primate brain using transcranial focused ultrasound stimulation. Neuron 2019;101:1109−16. e5.

[11] Fouragnan EF, Chau BKH, Folloni D, Kolling N, Verhagen L, Klein-Flügge M, Tankelevitch L, Papageorgiou GK, Aubry J-F, Sallet J, Rushworth MFS. The macaque anterior cingulate cortex translates counterfactual choice value into actual behavioral change. Nat Neurosci 2019;22:797−808.

[12] Legon W, Ai L, Bansal P, Mueller JK. Neuromodulation with single-element transcranial focused ultrasound in human thalamus. Hum Brain Mapp 2018;39:1995−2006.

[13] Badran BW, Caulfield KA, Stomberg-Firestein S, Summers PM, Dowdle LT, Savoca M, Li X, Austelle CW, Short EB, Borckardt JJ, Spivak N, Bystritsky A, George MS. Sonication of the anterior thalamus with MRI-Guided transcranial focused ultrasound (tFUS) alters pain thresholds in healthy adults: a double-blind, sham-controlled study. Brain Stimul 2020;13:1805−12.

[14] Ozenne V, Constans C, Bour P, Santin MD, Valabrègue R, Ahnine H, Pouget P, Lehéricy S, Aubry J-F, Quesson B. MRI monitoring of temperature and displacement for transcranial focus ultrasound applications. Neuroimage 2020;204:116236.

[15] Phipps MA, Jonathan SV, Yang P-F, Chaplin V, Chen LM, Grissom WA, Caskey CF. Considerations for ultrasound exposure during transcranial MR acoustic radiation force imaging. Sci Rep 2019;9:16235.

[16] Xu Z, Carlson C, Snell J, Eames M, Hananel A, Lopes MB, Raghavan P, Lee C-C, Yen C-P, Schlesinger D, Kassell NF, Aubry J-F, Sheehan J. Intracranial inertial cavitation threshold and thermal ablation lesion creation using MRI-guided 220-kHz focused ultrasound surgery: preclinical investigation. J Neurosurg 2015;122:152−61.

[17] ter Haar G. Ultrasound bioeffects and safety. Proc Inst Mech Eng H 2010;224: 363−73.

[18] Constans C, Mateo P, Tanter M, Aubry J-F. Potential impact of thermal effects during ultrasonic neurostimulation: retrospective numerical estimation of temperature elevation in seven rodent setups. Phys Med Biol 2018;63: 025003.

[19] Sapareto SA, Dewey WC. Thermal dose determination in cancer therapy. Int J Radiat Oncol Biol Phys 1984;10:787−800.

[20] Lee M, Schlesinger D, ter Haar G, Sela B, Eames M, Snell J, Hananel A, Kassell N, Sheehan J, Larner J. Thermal dose and radiation dose comparison based on cell survival. J. Therapeutic Ultrasound 2015;3:P26.

[21] Hynynen K, Vykhodtseva NI, Chung AH, Sorrentino V, Colucci V, Jolesz FA. Thermal effects of focused ultrasound on the brain: determination with MR imaging. Radiology 1997;204:247−53.

[22] Gateau J, Aubry J-F, Chauvet D, Boch A-L, Fink M, Tanter M. In vivo bubble nucleation probability in sheep brain tissue. Phys Med Biol 2011;56:7001−15.

[23] Apfel RE, Holland CK. Gauging the likelihood of cavitation from short-pulse, low-duty cycle diagnostic ultrasound. Ultrasound Med Biol 1991;17:179−85.

[24] Crum LA, Roy RA, Dinno MA, Church CC, Apfel RE, Holland CK, Madanshetty SI. Acoustic cavitation produced by microsecond pulses of ultrasound: a discussion of some selected results. J Acoust Soc Am 1992;91:1113−9.

[25] Bailey MR, Pishchalnikov YA, Sapozhnikov OA, Cleveland RO, McAteer JA, Miller NA, Pishchalnikova IV, Connors BA, Crum LA, Evan AP. Cavitation detection during shock-wave lithotripsy. Ultrasound Med Biol 2005;31: 1245−56.

[26] Gateau J, Taccoen N, Tanter M, Aubry J-F. Statistics of acoustically induced bubble-nucleation events in in vitro blood: a feasibility study. Ultrasound Med Biol 2013;39:1812−25.

[27] C. for D. and R. Health. Marketing clearance of diagnostic ultrasound systems and transducers. U.S. Food and Drug Administration; 2019. available at, https://www.fda.gov/regulatory-information/search-fda-guidance-documents/marketing-clearance-diagnostic-ultrasound-systems-and-transducers).

[28] Holland CK, Apfel RE. Fundamentals of the mechanical Index and caveats in its application. J Acoust Soc Am 1999;105:1324. −1324.

[29] Pinton GF, Aubry J-F, Fink M, Tanter M. Numerical prediction of frequency dependent 3D maps of mechanical index thresholds in ultrasonic brain therapy. IEEE; 2010. p. 2258−61.

[30] Fry FJ, Barger JE. Acoustical properties of the human skull. J Acoust Soc Am 1978;63:1576−90.

[31] Pinton G, Aubry J-F, Bossy E, Muller M, Pernot M, Tanter M. Attenuation, scattering, and absorption of ultrasound in the skull bone: absorption of ultrasound in the skull bone. Med Phys 2011;39:299−307.

[32] Hayner M, Hynynen K. Numerical analysis of ultrasonic transmission and absorption of oblique plane waves through the human skull. J Acoust Soc Am 2001;110:3319−30.

[33] Pichardo S, Sin VW, Hynynen K. Multi-frequency characterization of the speed of sound and attenuation coefficient for longitudinal transmission of freshly excised human skulls. Phys Med Biol 2011;56:219−50.

[34] Eames MD, Hananel A, Snell JW, Kassell NF, Aubry J-F. Trans-cranial focused ultrasound without hair shaving: feasibility study in an ex vivo cadaver model. J. Therapeutic Ultrasound 2014;1:1−6.

[35] Kinsler LE. Fundamentals of acoustics. New York: Wiley; 1982.

[36] Cobbold RS. Foundations of biomedical ultrasound. Oxford university press; 2006.

[37] Chen J, LeBlang S, Hananel A, Aginsky R, Perez J, Gofeld M, Shir Y, Aubry JF. An incoherent HIFU transducer for treatment of the medial branch nerve: numerical study and in vivo validation. Int J Hyperther 2020;37:1219−28.

[38] Leung SA, Webb TD, Bitton RR, Ghanouni P, Butts Pauly K. A rapid beam simulation framework for transcranial focused ultrasound. Sci Rep 2019;9: 7965.

[39] Robertson J, Martin E, Cox B, Treeby BE. Sensitivity of simulated transcranial ultrasound fields to acoustic medium property maps. Phys Med Biol 2017;62: 2559−80.

[40] White PJ, Clement GT, Hynynen K. Longitudinal and shear mode ultrasound propagation in human skull bone. Ultrasound Med Biol 2006;32:1085−96.

[41] Yousefian O, Karbalaeisadegh Y, Muller M. Frequency-dependent analysis of ultrasound apparent absorption coefficient in multiple scattering porous media: application to cortical bone. Phys Med Biol 2021;66:035026.

[42] Duck FA. Physical properties of tissues: a comprehensive reference book. London: Academic Press Inc; 1990.

[43] Chauvet D, Marsac L, Pernot M, Boch A-L, Guillevin R, Salameh N, Souris L, Darrasse L, Fink M, Tanter M, Aubry J-F. Targeting accuracy of transcranial magnetic resonance-guided high-intensity focused ultrasound brain therapy: a fresh cadaver model. J Neurosurg 2013;118:1046−52.

[44] Otsu N. A threshold selection method from gray-level histograms. IEEE Transact Syst Man Cybernetics 1979;9:62–6.

[45] Lillie EM, Urban JE, Lynch SK, Weaver AA, Stitzel JD. Evaluation of skull cortical thickness changes with age and sex from computed tomography scans. J Bone Miner Res 2016;31:299–307.

[46] Peterson J, Dechow PC. Material properties of the human cranial vault and zygoma. Anat Rec A Discov Mol Cell Evol Biol 2003;274:785–97.

[47] Li H, Ruan J, Xie Z, Wang H, Liu Wengling. Investigation of the critical geometric characteristics of living human skulls utilising medical image analysis techniques. Int J Veh Saf 2007;2:345–67.

[48] ANSI/AAMI HE75. (R2018) - human factors engineering - design of medical devices. 2009.

[49] Riis TS, Webb TD, Kubanek J. Acoustic properties across the human skull. Ultrasonics 2022;119:106591.

[50] Marsac L, Chauvet D, La Greca R, Boch A-L, Chaumoitre K, Tanter M, Aubry J-F. Ex vivo optimisation of a heterogeneous speed of sound model of the human skull for non-invasive transcranial focused ultrasound at 1 MHz. Int J Hyperther 2017;33:635–45.

[51] Gimeno LA, Martin E, Wright O, Treeby BE. Experimental assessment of skull aberration and transmission loss at 270 kHz for focused ultrasound stimulation of the primary visual cortex. In: 2019 IEEE international ultrasonics symposium (IUS); 2019. p. 556–9.

[52] M. Chen, C. Peng, H. Wu, C.-C. Huang, T. Kim, Z. Traylor, M. Muller, P. Y. Chhatbar, C. S. Nam, W. Feng, X. Jiang, Numerical and experimental evaluation of low-intensity transcranial focused ultrasound wave propagation using human skulls for brain neuromodulation. Med Phys. **n/a**, doi:10.1002/mp.16090.

[53] Baron C, Aubry J-F, Tanter M, Meairs S, Fink M. Simulation of intracranial acoustic fields in clinical trials of sonothrombolysis. Ultrasound Med Biol 2009;35:1148–58.

[54] Marquet F, Pernot M, Aubry JF, Montaldo G, Marsac L, Tanter M, Fink M. Non-invasive transcranial ultrasound therapy based on a 3D CT scan: protocol validation and in vitro results. Phys Med Biol 2009;54:2597–613.

[55] Sun J, Hynynen K. The potential of transskull ultrasound therapy and surgery using the maximum available skull surface area. J Acoust Soc Am 1999;105:2519–27.

[56] Braun V, Blackmore J, Cleveland RO, Butler CR. Transcranial ultrasound stimulation in humans is associated with an auditory confound that can be effectively masked. Brain Stimul 2020;13:1527–34.

[57] White J, Clement GT, Hynynen K. Transcranial ultrasound focus reconstruction with phase and amplitude correction. IEEE Trans Ultrason Ferroelectrics Freq Control 2005;52:1518–22.

[58] Aubry J-F, Tanter M, Pernot M, Thomas J-L, Fink M. Experimental demonstration of noninvasive transskull adaptive focusing based on prior computed tomography scans. J Acoust Soc Am 2003;113:84–93.

[59] Maimbourg G, Houdouin A, Deffieux T, Tanter M, Aubry J-F. 3D-printed adaptive acoustic lens as a disruptive technology for transcranial ultrasound therapy using single-element transducers. Phys Med Biol 2018;63:025026.

[60] Fomenko A, Chen K-HS, Nankoo J-F, Saravanamuttu J, Wang Y, El-Baba M, Xia X, Seerala SS, Hynynen K, Lozano AM, Chen R. Systematic examination of low-intensity ultrasound parameters on human motor cortex excitability and behavior. Elife 2020;9:e54497.

[61] Ai L, Mueller JK, Grant A, Eryaman Y, Legon W. Transcranial focused ultrasound for BOLD fMRI signal modulation in humans. In: 2016 38th annual international conference of the IEEE engineering in medicine and biology society. EMBC); 2016. p. 1758–61.

[62] Ai L, Bansal P, Mueller JK, Legon W. Effects of transcranial focused ultrasound on human primary motor cortex using 7T fMRI: a pilot study. BMC Neurosci 2018;19:56.

[63] Cain JA, Spivak NM, Coetzee JP, Crone JS, Johnson MA, Lutkenhoff ES, Real C, Buitrago-Blanco M, Vespa PM, Schnakers C, Monti MM. Ultrasonic thalamic stimulation in chronic disorders of consciousness. Brain Stimul: Basic, Translational, and Clinical Research in Neuromodulation 2021;14:301–3.

[64] Itrusst," (available at https://itrusst.github.io/).